ACS OMEGA

Article

Cite This: ACS Omega 2018, 3, 4400−4411

Improving the Impact Strength and Heat Resistance of 3D Printed Models: Structure, Property, and Processing Correlationships during Fused Deposition Modeling (FDM) of Poly(Lactic Acid)

Claire Benwood,[†] Andrew Anstey,[†] Jacek Andrzejewski,[†,§] Manjusri Misra,*[,†,‡] and Amar K. Mohanty*[,†,‡]

[†]Bioproducts Discovery and Development Centre, Department of Plant Agriculture, University of Guelph, Crop Science Building, Guelph ON N1G 2W1, Ontario, Canada

[‡]School of Engineering, University of Guelph, Thornbrough Building, Guelph ON N1G 2W1, Ontario, Canada

[§]Polymer Processing Division, Institute of Materials Technology, Faculty of Mechanical Engineering and Management, Poznan University of Technology, Piotrowo 3 Street, Poznan 61-138, Poland

ABSTRACT: A fused deposition modeling method was used in this research to investigate the possibility of improving the mechanical properties of poly(lactic acid) by changing the thermal conditions of the printing process. Sample models were prepared while varying a wide range of printing parameters, including bed temperature, melt temperature, and raster angle. Certain samples were also thermally treated by annealing. The prepared materials were subjected to a detailed thermomechanical analysis (differential scanning calorimetry, dynamic mechanical analysis, heat deflection temperature (HDT)), which allowed the formulation of several conclusions. For all prepared samples, the key changes in mechanical properties are related to the content of the poly(lactic acid) crystalline phase, which led to superior properties in annealed samples. The results also indicate the highly beneficial effect of increased bed temperature, where the best results were obtained for the samples printed at 105 °C. Compared to the reference samples printed at a bed temperature of 60 °C, these samples showed the impact strength increased by 80% (from 35 to 63 J/m), HDT increased by 20 °C (from 55 to 75 °C), and also a significant increase in strength and modulus. Scanning electron microscopy observations confirmed the increased level of diffusion between the individual layers of the printed filament.

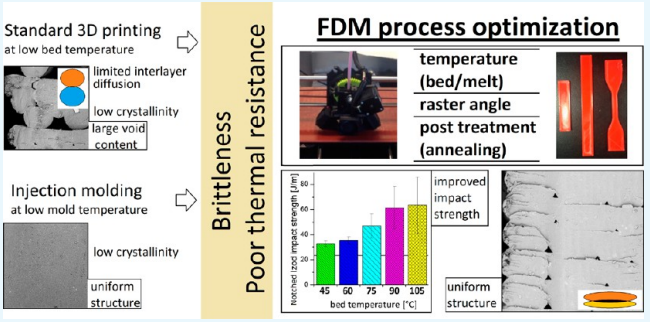

INTRODUCTION

Fused deposition modeling (FDM) is a type of three-dimensional (3D) printing where a thermoplastic filament is heated above the melting temperature and then extruded onto a print surface in layers. It is applicable to many industries including healthcare, transportation, housing, and farming, as well as a variety of industrial applications where there is a benefit from the customization of individual items.[1,2] The many benefits of FDM include promoting sustainable, inexpensive development with decreased material waste, eliminating tooling requirements, and a significantly shorter supply chain.[1,2] The costs of 3D printers are decreasing, resulting in increased home usage and the need to better understand the properties of the material being printed, specifically for load-bearing purposes.[1] FDM is currently undergoing a transition from rapid prototyping to rapid manufacturing. For that reason, new materials, equipment, and manufacturing procedures need to be developed further.[3]

Poly(lactic acid) (PLA) is a biobased, compostable, thermoplastic polyester obtained from annually renewable resources such as corn or sugar beets.[4] PLA has the potential to replace petroleum-based thermoplastics, and its low melting point is a major benefit as it requires less energy to 3D print compared to that for acrylonitrile butadiene styrene (ABS) and polyamides.[5,6] PLA has a number of diverse uses, including biomedical and industrial applications. Its biocompatible and bioresorbable properties provide many biomedical opportunities, and its good mechanical properties and compostability are well-suited for industrial applications.[4,7] Different crystal structures and degrees of crystallinity can be developed by varying the thermal history of the material, which allows for different properties to be tailored depending on the application.[5−8]

The significant effect of process parameters on the mechanical properties of the samples created using FDM has been extensively studied using acrylonitrile butadiene styrene (ABS) filaments. Because of the relatively long process time, selected process parameters can be monitored in real time. An

Received: January 22, 2018
Accepted: March 28, 2018
Published: April 23, 2018

DOI: 10.1021/acsomega.8b00129
ACS Omega 2018, 3, 4400−4411

example of this type of in-line measurements is the utilization of fiber Bragg grating sensors.[9] Simultaneous observation of the stress field and temperature allows the evaluation of the inter-/intralayer adhesion and distortion between the rasters, structural inhomogeneity, and thermal history. These factors have a significant impact on the mechanical properties of the finished parts.[9−12] Highly anisotropic properties were proven to be a function of how FDM extrudes the filament onto the print surface in layers.[13,14] Process parameters including orientation, layer thickness, raster angle, raster width, air gap, processing temperature, and layout of samples on the print surface were studied to determine their effect on the mechanical properties of the ABS samples, and the results were used to optimize the parameters and greatly improve the mechanical properties of the 3D printed parts.[10,11,14,15]

Studies concerning PLA and the relationship between its crystallinity and mechanical properties have also been conducted. Harris and Lee[4] investigated how manipulating the process parameters, specifically increasing the annealing time of injection-molded PLA, would impact the crystallinity and in turn the mechanical properties of their samples. They found that optimizing the molding cycle as well as adding nucleating agents enhanced the crystallinity by 37%, resulting in an increase in flexural strength and modulus by 25% and heat deflection temperature (HDT) by 30 °C. In addition, constant crystallinity was observed throughout the parts after annealing.[4] Wang et al.[6] also observed in their study of FDM that an increase in crystallinity of 3D printed PLA corresponded to a high impact strength.[6] Drummer et al.[16] investigated FDM of PLA filled with tricalcium phosphate. They found that a greater extruder temperature resulted in increased crystallinity partially because previous layers deposited and bonded together were reheated by new filaments being extruded nearby. This was also observed to affect the tensile strength of the samples.[16]

Many different process parameters in regard to FDM of PLA have been studied. These include the build orientation, layer thickness, feed rate, plate temperature, uniaxial direction of rasters, distance between filaments, extruder temperature, and color. All were found to have varying degrees of impact on the mechanical properties of 3D printed PLA.[5,17−20] Tymrak et al.[19] quantified the tensile strength and elastic modulus of PLA 3D printed under realistic environmental conditions on RepRap printers. Process parameters were not defined, and it was observed that the variety of different settings utilized had a large effect on the structure and properties of the samples. A high extruder temperature was found to result in increased thermal bonding and inter-/intralayer lamination and resulted in a higher tensile strength.[19] Variation in the unidirectional raster orientation has also been studied with regard to FDM of PLA and was found to alter the mechanical properties of the parts. In one case, the ultimate tensile strength increased 55% with the change in raster angle.[20−22] The effect of annealing on the crystallinity of the 3D printed PLA parts was briefly reviewed, with results indicating no change when the printed samples were annealed below the T_g; however, a reduction in strength between 10 and 30% was observed.[22]

The majority of research concerning the impact of printing parameters on the mechanical properties of 3D printed components usually focuses on ABS-based materials, analyzing the impact of a wide spectrum of variables and predicting properties based on numerical simulations.[23−25] In addition to the most frequently analyzed machine parameters, such as nozzle diameter, layer orientation, or printing speed, PLA-related research also often includes temperature parameters and additional thermal treatment.[22,26] The main goal of the presented research was a comprehensive assessment of the most important factors from each of the parameter categories to provide a reliable evaluation of the benefits. On the basis of literature sources, the selection of variable parameters included the temperature of the printer nozzle and bed. The raster angle orientation was chosen as the main machine factor. Annealing treatment was chosen as the additional process-independent factor. For verification and comparative purposes, injection-molded samples were also prepared.

RESULTS AND DISCUSSION

Correlation of Thermal Parameters with the Density of FDM-Printed Samples. The viscosity graphs shown in Figure 1 present the results of the frequency sweep measurements at various temperatures. Rheological tests can confirm only the viscosity changes occurring within the printing nozzle, which do not translate into real material viscosity after leaving the nozzle. In addition, it can be noted that any increase in print temperature can lead to the intensification of degradation phenomena, which is evident from the reducing viscosity in the low deformation frequency range. In the case of FDM techniques, these changes have a negligible effect on material degradation because the residence time of the material in the nozzle is very short. Even at temperatures significantly greater than the recommended printing conditions, it does not usually lead to visible changes in the quality of the model, which has also been confirmed by other researchers.[27] This is primarily due to the very nature of the FDM printing method, as the material flowing from the nozzle, even with a significant reduction in viscosity, is rapidly cooled down when it comes in contact with the ground surface.

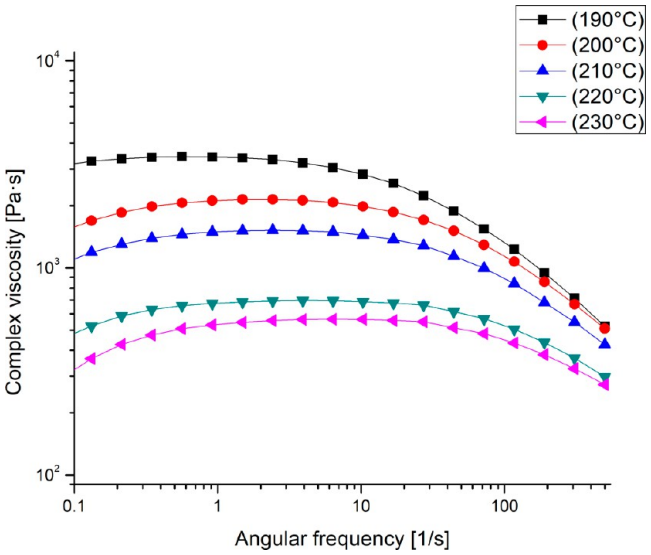

Figure 1. Complex viscosity plot measured at different temperatures, reflecting the variations of the printing nozzle temperature.

Dimensional accuracy of the FDM models also largely depends on the viscosity of the material used; in this case, the viscosity decrease usually has a negative impact on the model mapping, which is related to the inability to accurately controlling the height of the extruded material path. However, the high viscosity that allows for a proper control of the layer

DOI: 10.1021/acsomega.8b00129
ACS Omega 2018, 3, 4400−4411

height of the model also increases the content of free spaces between the paths. The 3D model structure shown in Figure 2

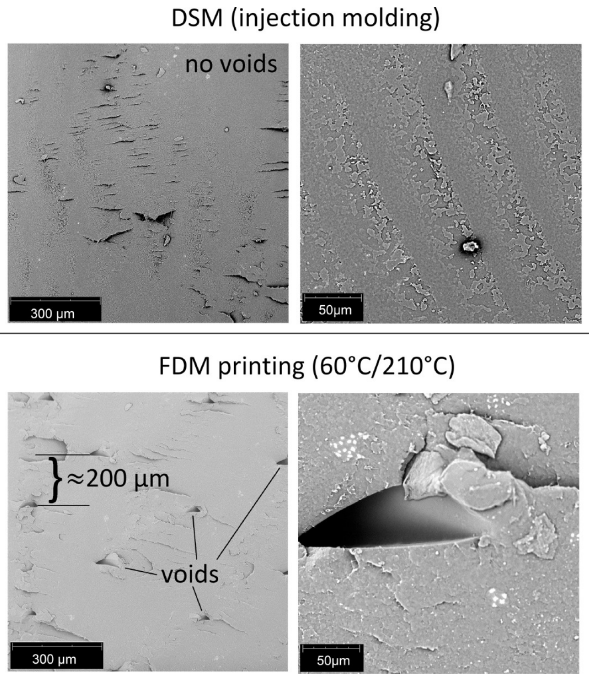

Figure 2. Appearance of the sample structure after injection molding processing and under optimal conditions of the FDM printing process.

presents the sample prepared at the parameters optimized to obtain the high dimensional accuracy of the model (bed temp = 60 °C; melt temp = 210 °C). The proper selection of the printing parameters is indicated by the constant distance of 200 μm between the successive voids. These voids occur at the intersection of consecutive layers, and the distance between them corresponds to the height of a single layer of the deposited filament given by the printer program.

Unlike conventional polymer processing techniques such as extrusion and injection molding, FDM printing does not allow for a wide variation of the flow characteristics through appropriate parameter selection. The viscosity of the polymer melt depends mainly on the temperature gradient between the print nozzle and the surface of the rising model. Most commonly used 3D printers offer the ability to controlling only the bed and nozzle temperatures, which simply leads to the need for multiple comparative tests to optimize the range of both temperature variations.[10] Because the temperature range of both the melt and bed was relatively wide in the presented studies, changes in these parameters also caused changes in the degree of filling of the resulting sample models. The density values presented in Figure 3 show a comparison of the specific density measurements for samples printed at variable bed and nozzle temperatures. These results are also confirmed by the scanning electron microscope (SEM) picture presented in the same figure; the discussed images represent printed samples prepared at extremely different bed temperatures, 45 and 105 °C, respectively. The results confirmed the more significant consequences of bed temperature changes on the model's filling level. Similar conclusions were formulated by Wang et al.;[6] however, in their research, the bed temperature was the main variable and the temperature range was very high (from 30 to 160 °C).

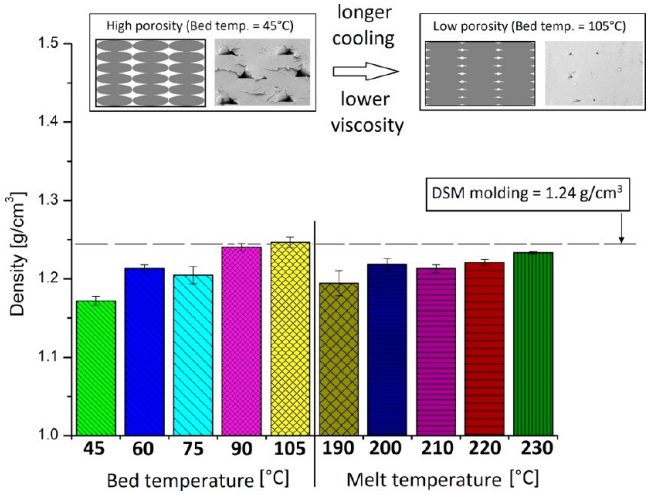

Figure 3. Density variations for different thermal conditions in the printing process. The picture comparison reflects the raster area cross section from high-porosity samples (bed temperature of 45 °C) and low-porosity samples (bed temperature of 105 °C).

In the case of density analysis, it is worth mentioning that for most of the parts printed with FDM techniques the filling density is often reduced in a targeted manner to reduce the material consumption and also the dimension accuracy.[28] This modification occurs by reducing the density of the model's filing mesh, while maintaining the solid structure of the shell layer. With such a constructed model, it is of course not possible to obtain the maximum possible strength of the samples, but taking into account the significant mass reduction, this operation has many advantages.

Taking into account the main objective of the research, which is to increase the mechanical performance of PLA-based 3D models, the porosity (void content) measured during the density measurements was only 5.5% in the worst case of samples printed at the bed temperature of 45 °C. Surprisingly, the density of the samples printed at the highest bed temperature (90 and 105 °C) does not differ from the values obtained for injection-molded samples, which proves not only very small porosity content but also confirms the density changes of PLA itself caused by increased crystallinity, which was observed for PLA previously.[29] According to numerous studies,[30,31] the density of fully amorphous PLA is 1.248 g/cm^3, whereas that of 100% crystalline PLA is 1.290 g/cm^3, which may confirm the unexpected increase in specific density for selected samples.

Differential Scanning Calorimetry (DSC) Measurements: Crystallinity Evaluation. Differential scanning calorimetry (DSC) was employed to determine the degree of crystallinity of the FDM samples as well as to gain an insight into the influence of sample thermal history on basic thermomechanical properties. The changes in the crystallinity level for printed samples can be seen in Figure 4; the basic thermal properties are listed in Table 1.

It can be seen from Figure 5 that the variation of the print temperature of the samples did not have a significant effect on the crystallinity or the melting peak. Some visible changes can be considered as negligible because they do not show any trend and generally are within the range of measurement error. Although crystallization half time ($t_{1/2}$) decreases as the crystallization temperature (T_c) increases, with the crystal growth rate considered proportional, this has been reported to

DOI: 10.1021/acsomega.8b00129
ACS Omega 2018, 3, 4400−4411

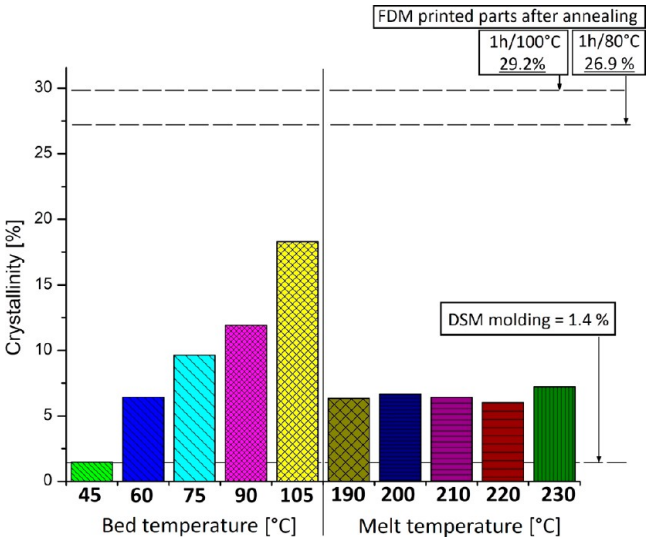

Figure 4. Comparison of crystallinity degrees for samples printed with different thermal conditions and injection-molded samples (DSM).

Table 1. Thermal Properties of PLA-Based Samples

	1st heating			2nd heating
	enthalpy (J/g)			
sample	ΔH_{cc}	ΔH_m	crystallinity (%)	crystallinity (%)
injection molded	24.9	26.3	1.44	22.11
Bed Temperature (°C)				
45 °C	22.7	26.1	1.48	21.19
60 °C	22.0	28.4	6.41	22.51
75 °C	18.5	27.5	9.62	23.40
90 °C	13.4	24.5	11.92	23.80
105 °C	7.7	24.9	18.30	21.08
Melt Temperature (°C)				
190 °C	20.3	26.3	6.32	23.87
200 °C	22.3	28.5	6.65	24.72
210 °C	22.1	28.1	6.41	25.61
220 °C	22.1	27.7	6.00	25.88
230 °C	22.1	28.9	7.21	25.37
Annealing (°C)				
80 °C		25.2	26.89	29.19
100 °C		27.4	29.24	29.40

be true only up to around 110 °C for pure PLA. At this point, the crystallization process becomes slower as the T_c increases, which was observed by Sánchez et al.[32] in a series of measurements of PLA crystallization kinetics. Although the print temperatures are much higher than the boundary temperature of 110 °C, the temperature fluctuation from the extruded filament and the rapid cooling after deposition do not keep the filament at the elevated temperature long enough for a significant difference in crystallinity to occur. This has in turn been reported in other studies, when bed temperatures reached 160 °C (close to the PLA melting point).[6] The presence of a small double melting peak in the DSC signal can be observed for most of the samples. This is a result of the α' crystal structure melting and then recrystallizing into its α form with tighter and more ordered chain packing; this phenomenon is quite widely described by di Lorenzo et al.[33] for PLA-based materials.[34,35] Because there are so few α crystal structures as assumed from the very slight melting peak, the elongation at break and the modulus of the samples were not seen to be

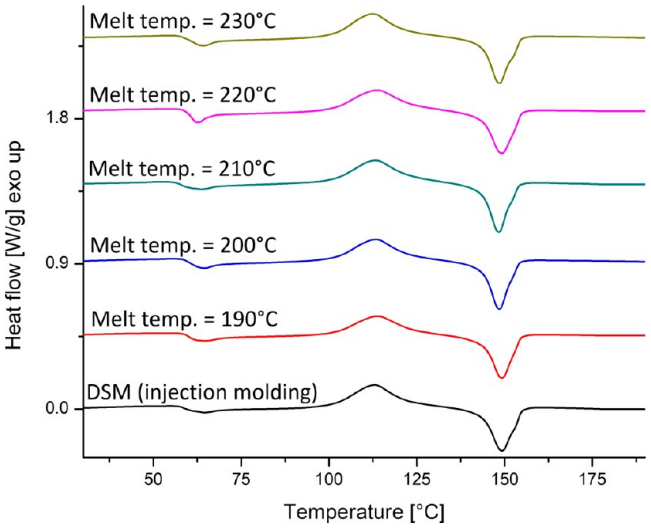

Figure 5. Comparison of the DSC curves obtained from the 1st heating stage for PLA samples printed at different melt temperatures and injection-molded PLA.

affected. All of the samples printed at varying print temperatures had no significant changes in their mechanical properties, apart from the samples printed at a temperature of 190 °C. This indicates that although having the same degree of crystallinity as that of the other samples there are other factors involved in determining the mechanical properties of the samples. The bonding between the filaments is also affected by the thermal history of the samples, and unsatisfactory bond strength between the filaments will lead to poor mechanical properties, regardless of the degree of crystallinity the sample has obtained. Because the filament diameter was so small, the printing temperature was seen to have a negligible effect on the crystallinity, as well as the mechanical properties of the samples (apart from the lowest print temperature).[12]

As seen in Figure 6, varying the bed temperature of the FDM samples had a significant effect on their degree of crystallinity achieved, cold crystallization, and melting peak. The cold crystallization peak enthalpy was reduced greatly as the bed

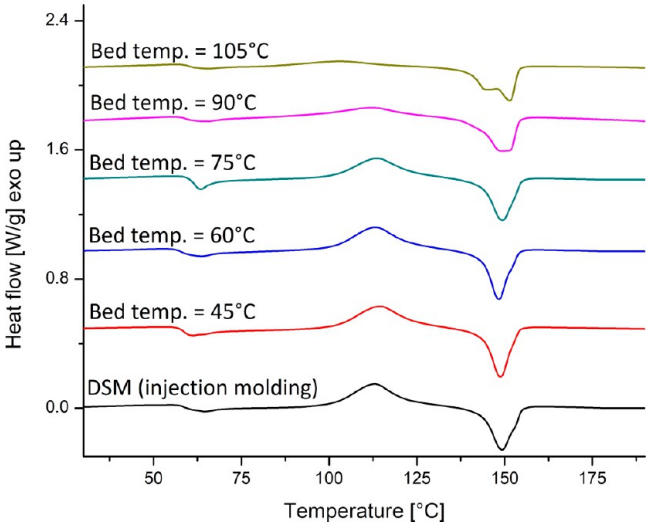

Figure 6. Comparison of the DSC curves obtained from the 1st heating stage for PLA samples printed at different bed temperatures and injection-molded PLA.

DOI: 10.1021/acsomega.8b00129
ACS Omega 2018, 3, 4400−4411

temperature increased gradually from 45 to 105 °C, indicating the increase in sample crystallinity. Also, the transition from α' to α crystals could be observed as the bed temperature increased. Up to the bed temperature of 75 °C, the shape of the DSC curves remain similar with a sharp melting peak at around 150 °C. Visible changes are observed for the sample printed at 90 °C, where top of the melting peak is clearly flattened, which is potentially the result of the convolution of two melting peaks. Two clearly defined melting peaks appear for samples printed at 105 °C; this phenomenon, already described in the literature, indicates the existence of two separate crystalline structures, formed as a result of different crystallization kinetics.[32,36] A large increase in overall crystallinity was observed for the whole observed range of bed temperature from 45 to 105 °C. The crystallinity level of 1.5% reported for the samples printed at the lowest bed temperature of 45 °C is most similar to the value obtained for injection-molded samples. The greater impact of bed temperature changes could be a result of shifting the crystallization regimes. This gradual change in crystallization kinetics, described in detail by Saeidlou et al.,[7] is associated with a favorable transition of thermodynamic conditions from regime III (where the low chain motion limits the lamella growth) to regime II (where the crystal growth occurs from prolific multiple nucleation at a lower temperature, resulting in a faster crystallization process). For PLA samples, this transition phenomenon has been reported to occur at around 120 °C but again, with the fluctuating temperature cycles and the print temperature decreasing rapidly, it is difficult to say the exact average temperature each print achieved. The change of regimes promotes increased and faster crystallization, as evidenced by the increase in crystallinity.[7] The regime change and growth of two crystal structures were found to occur at the same temperature and are both associated with the double melting peak.

Although the increased bed temperature caused a significant increase in crystallinity and mechanical properties, this effect may be lost in the case of printing real models. Because of their geometry and size, it would be difficult to maintain identical thermal conditions of printing, as is the case with research samples. This problem is indicated by numerous studies,[37,38] especially because this problem concerns not only the level of crystallinity but also an equally important issue regarding the weld formation of individual model layers.[39,40] The role of these factors becomes even more important if we take into account the growing importance of large-scale additive manufacturing technology, where the maximum size of printed elements reaches several meters, which causes numerous problems related to the need to ensure thermal stability on such a large scale.[41,42] The classical solution to most of the problems related to the heterogeneity of the 3D model structure is post-processing. For PLA especially, annealing allows us to obtain measurable benefits, especially in the context of improving mechanical properties.[6,22] Post-print annealing was done to observe the effects on the samples and to evaluate whether it would be a viable method of obtaining the same outcomes on parts with different dimensions. Different variations of 3D printers for FDM exist and include models with the print area in an enclosed space with the option to adjust the ambient temperature.

Two sets of samples 3D printed at a bed temp of 60 °C and print temperature of 200 °C were annealed at 80 and 100 °C for 1 h each. Harris and Lee found that annealing longer did not increase the crystallinity after 1 h (annealed at 80 °C).[4] The maximum crystallinity of PLA is reported to be just below 45%; however, the maximum crystallinity achieved with the studied samples was around 30%. There was not a significant increase in crystallinity between the two different annealing temperatures (see Figure 7); however, the appearance of the melting

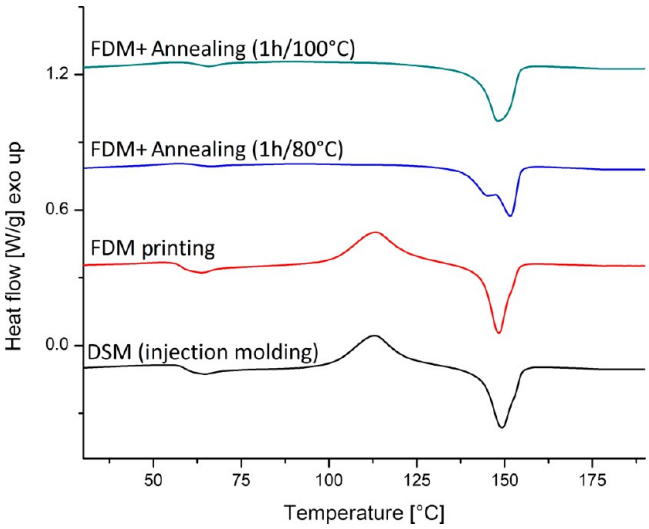

Figure 7. Comparison of the DSC 1st heating curves for injection-molded samples and FDM-printed specimens before and after annealing.

peaks was quite different. The 80 °C annealed sample displayed a double melting peak, indicating the formation of two different crystalline structures, α and α'. The 100 °C annealed sample had a single wide peak; perhaps, the two melting peaks were superimposed, indicating that there were more α crystals formed. Further supporting that theory, when observing the mechanical properties, the mechanical properties are quite different despite only a small difference in crystallinity.

The injection-molded sample displayed low crystallinity. This was mainly due to the fact that the grades of PLA used in 3D printing are intended mainly for the production of film,[43] which in the end improves the dimensional stability of the products by reducing the shrinkage but also reveals the majority of defects caused by the amorphous structure of the material. Cold crystallization and a single melting peak of prepared samples indicated that there were only α prime crystals formed during this process. Despite being one of the samples with the lowest degree of crystallinity, all of the mechanical properties displayed were among the highest with the exception of the notched Izod impact strength, which was similar to that of samples 3D printed at lower bed temperatures.[19,28]

Mechanical Tests. The values of the basic mechanical parameters obtained from static tensile/flexural testing and impact resistance measurements are collected in Table 2. Most important changes in the strength and modulus followed similar trends, both in tensile and flexural tests (see Figure 8).

In the case of printed samples, changes in mechanical properties follow the increase in the crystallinity of PLA; this is evident for samples printed at constant nozzle and variable bed temperatures. In the case of variable nozzle temperature, changes in strength and modulus were not so evident because the content of crystalline phase for this group of samples does not change significantly. The comparative analysis of the 3D printed, molded, and annealed samples is presented in Figure 9

DOI: 10.1021/acsomega.8b00129
ACS Omega 2018, 3, 4400−4411

Table 2. Mechanical Properties of All Prepared PLA-Based Samples from Tensile, Flexural, and Izod Impact Measurements

	tensile test				flexural test		Izod test
sample	modulus (MPa)	strength (MPa)	elongation at yield (%)	elongation at break (%)	modulus (MPa)	strength (MPa)	impact strength (J/m)
injection molded	3223 (±122)	63.5 (±1.2)	2.6 (±0.14)	72.6 (±42.0)	3864 (±118)	103.3 (±1.9)	23.5 (±9.1)
Bed Temperature (°C)							
45 °C	2877 (±76.3)	54.2 (±1.3)	2.6 (±0.04)	5.49 (±0.85)	2314 (±78.9)	74.4 (±2.2)	32.8 (±2.4)
60 °C	3014 (±58.9)	62.0 (±1.0)	2.7 (±0.04)	7.45 (±3.0)	3002 (±157.4)	93.6 (±4.8)	35.5 (±2.7)
75 °C	3258 (±72.2)	60.7 (±1.4)	2.5 (±0.05)	4.58 (±0.95)	2927 (±169.1)	93.9 (±5.3)	47.2 (±9.5)
90 °C	3298 (±101.1)	64.1 (±0.9)	2.5 (±0.20)	5.34 (±0.85)	3217 (±131.0)	100.4 (±6.2)	61.6 (±16.9)
105 °C	3317 (±92.7)	65.9 (±2.0)	2.2 (±0.12)	4.98 (±1.2)	3529 (±236.0)	106.7 (±5.6)	63.4 (±22.6)
Melt Temperature (°C)							
190 °C	2748 (±123.9)	54.3 (±1.8)	2.7 (±0.13)	3.1 (±0.5)	2247 (±40.4)	71.7 (±2.1)	34.5 (±3.9)
200 °C	3105 (±38.2)	63.8 (±0.7)	2.8 (±0.06)	4.7 (±0.6)	3147 (±87.3)	98.7 (±4.0)	34.7 (±3.3)
210 °C	3014 (±58.9)	62.0 (±1.0)	2.7 (±0.04)	7.4 (±3.0)	3002 (±157.4)	93.6 (±4.8)	35.5 (±3.7)
220 °C	3040 (±95.3)	61.4 (±1.3)	2.5 (±0.06)	5.3 (±2.8)	2899 (±150.4)	94.3 (±4.6)	32.4 (±2.9)
230 °C	3032 (±67.1)	61.9 (±1.2)	2.6 (±0.12)	4.1 (±1.0)	3097 (±165.5)	97.1 (±3.7)	35.7 (±5.0)
Annealing (°C)							
80 °C	3360 (±102.5)	61.9 (±1.0)	2.5 (±0.3)	4.5 (±1.3)	3516 (±115.6)	103.9 (±3.0)	136.7 (±10.9)
100 °C	3334 (±162.3)	59.4 (±2.3)	2.4 (±0.2)	4.4 (±1.3)	3739 (±236.4)	109.4 (±6.4)	127.6 (±17.1)
Raster Angle (°)							
45/45°	3014 (±58.9)	62.0 (±1.0)	2.7 (±0.05)	7.4 (±3.0)	3002 (±157.4)	93.6 (±4.8)	35.5 (±2.7)
30/60°	3270 (±35.6)	61.5 (±1.8)	2.7 (±0.1)	3.6 (±0.9)	3175 (±99.3)	86.1 (±2.2)	32.9 (±1.1)
15/75°	3286 (±66.7)	62.5 (±1.1)	2.6 (±0.1)	3.7 (±0.3)	3215 (±214.0)	87.1 (±3.8)	33.1 (±4.6)
0/90°	3211 (±102.4)	61.5 (±2.2)	2.5 (±0.1)	3.7 (±1.0)	2974 (±123.5)	84.9 (±4.4)	30.9 (±2.3)

for tensile properties and in Figure 10 for flexural properties. Summarized results of elongation at break and impact resistance measurements are collected in Figure 11. From the comparison graphs, it can be seen that in the case of printed samples the rise in bed temperature from 60 to 105 °C causes a significant increase in mechanical properties. It is worth mentioning that this procedure results in comparable or even slightly higher mechanical properties than those obtained for injection-molded samples. This comparison also shows very favorable properties for annealed samples, both the modulus and the strength match the properties of the samples printed at the maximum bed temperature. However, an important advantage of annealing is a significant increase in impact strength compared to that of other printed samples (see Figure 12). It should be added here that the increase in impact strength is very significant, especially compared to that of injection-molded samples. Such a large difference indicates a very significant effect of the highly crystalline structures of the printed samples. Although in static measurements some predominance of the molded samples was visible, the impact tests confirm the great importance of the macromolecular structure formation, especially in the context of fracture mechanisms. This dependence has been already described in the literature also for PLA.[6,44−46] Along with thicker lamellae and ideal crystals, annealing can create different interlamellar regions, including the rigid amorphous phase and the mobile amorphous phase.[47,48] The injection-molded sample with a crystallinity of 1.5% had tensile properties very similar to those of the sample 3D printed at a bed temperature of 105 °C and a corresponding crystallinity of 18%. These results indicate that the tensile strength and modulus are dependent mostly on other factors, not just the degree of crystallinity. This is corroborated by the large variety of properties displayed in samples with similar crystallinities but different processing histories. Thermal bonding of filaments and crystal size may have contributed to this, as annealing creates larger crystals and temperature fluctuation was found to create smaller ones. Some sets of samples display a much higher standard deviation than others. This has been attributed to an unstable morphology where some of the polymer chains are more mobile than others, leading to a greater fluctuation in results.[48] Both the flexural strength and modulus increased with the increase in crystallinity. As was seen with the tensile properties, all of the samples with crystallinity of ∼5% have different flexural properties. The properties vary depending on the processing history, regardless of the degree of crystallinity. Unlike the tensile properties, the flexural modulus and strength both increase slightly with annealing.

The injection-molded samples had properties similar to those of the most promising 3D printed samples (FDM at a bed temperature of 105 °C), despite the large difference in crystallinity. The poor bonding between the filaments of the FDM samples was compensated by their favorable highly crystalline structure. The properties were comparable across all categories, with the exceptions of elongation at break values, where the injection-molded samples were higher. In turn, the notched Izod impact strength of the 3D printed samples was stronger. Both discrepancies can be attributed to the large difference in crystallinity, as increasing crystallinity has been shown to increase the impact strength as well as decrease the elongation at break.[6] A combination of low crystallinity and homogenous structure allowed the injection-molded sample to have a significantly greater maximum deformation than that of the FDM samples, in which elongation is mostly reduced because of stress concentration on the filament bonding surfaces.

The serious limitation related to the increasing temperatures of printing is dimensional stability; the samples began to warp and had difficulty adhering to the print surface.[49,50] Green painter's tape was applied to the print surface for samples printed at 90 and 105 °C to promote the adhesion of the samples to the print surface. Although there was significant

DOI: 10.1021/acsomega.8b00129
ACS Omega 2018, 3, 4400−4411

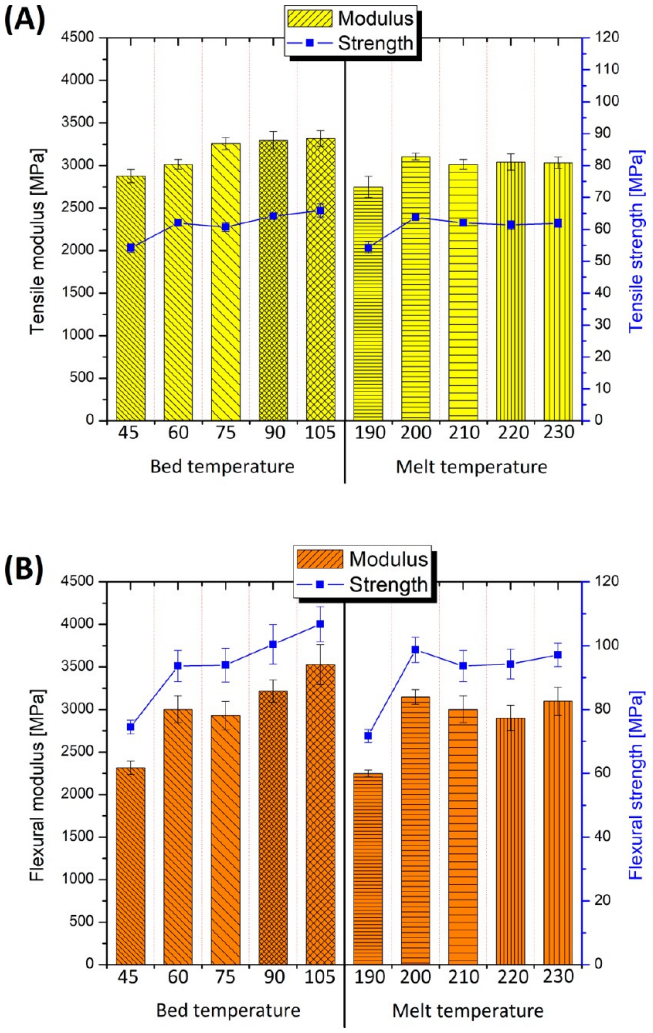

Figure 8. Tensile (A) and flexural (B) modulus/strength comparison for FDM-printed samples.

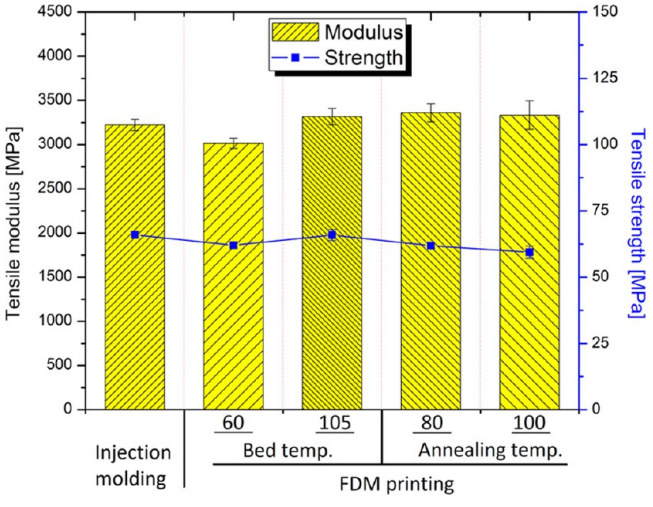

Figure 9. Comparison of tensile strength and modulus values for injection-molded samples and FDM-printed specimens at different bed temperatures and annealing treatments.

improvement in the adhesion, there was still some warping observed on a number of samples. This had a negligible effect on the mechanical properties; they still increased with the

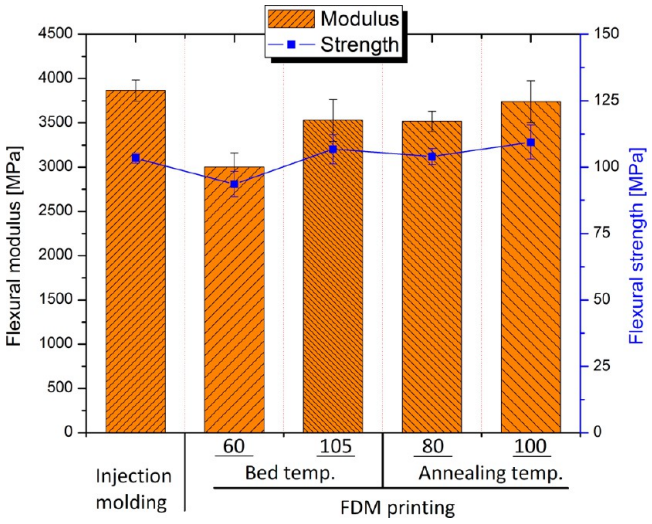

Figure 10. Comparison of flexural strength and modulus values for injection-molded samples and FDM-printed specimens at different bed temperatures and after annealing treatments.

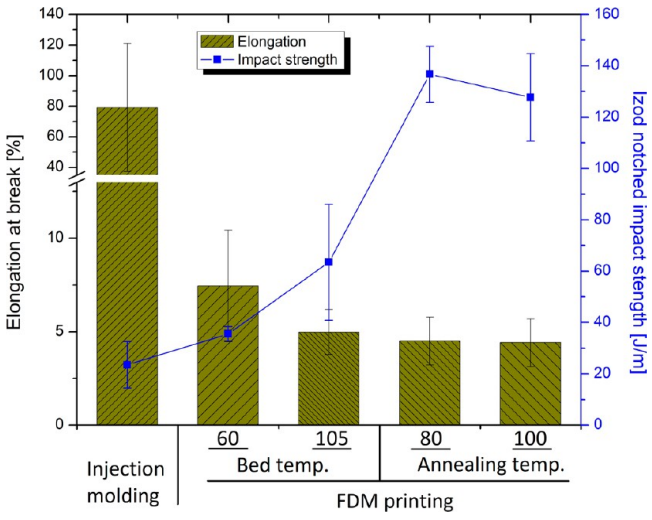

Figure 11. Elongation at break and notched Izod impact strength for injection-molded samples and FDM-printed specimens at different bed temperatures and after annealing treatments.

increasing crystallinity and bed temperatures. Depending on the quality of the surface finish and accuracy of dimensions required, it is not feasible to increase the bed temperature further with the current filament and print surface.

In previous studies,[21,51] the mechanical characteristics for a unidirectional raster angle were found to reduce when the raster angle was increased from 0 to 90°. The 90° angle was also observed to make the sample more brittle.[21] For this study, the 45/45° raster angle was overall the most consistent and stable of the angles. There was not a significant difference between most of the properties when compared. This is a result of the multidirectional nature of the filament in the sample. All previous studies were completed on unidirectional raster angles and, as a result, saw a much larger difference in properties. The flexural modulus was the only property where the 15/75 and 30/60° angles were superior.

Most of the values of strength and modulus for samples printed at 75 °C and above are very similar; taking into account the standard deviation values, these differences are negligible. In

DOI: 10.1021/acsomega.8b00129
ACS Omega 2018, 3, 4400−4411

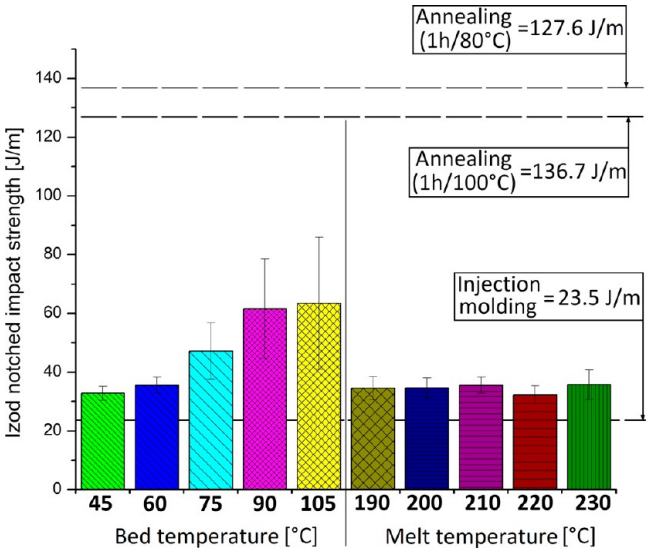

Figure 12. Impact resistance from the notched Izod measurements for FDM-printed samples under different thermal conditions.

our opinion, this is a beneficial behavior, especially taking into account that similar properties were obtained after injection molding of the same material. The mechanical characterization as presented in the article is aimed at highlighting the differences for samples printed with the use of heated printing bed and without it (such as for low-cost desktop printers). In contrast to impact strength, where the PLA crystallinity level is very important for results, most of the parameters obtained in static samples are very stable even for samples with different printing parameters.

Dynamic Mechanical Analysis (DMA) and Heat Deflection Temperature Changes. For most of the tested samples, the significant changes in mechanical characteristics are mainly caused by the changing content of the crystalline phase. This trend applies in particular to impact resistance. For PLA, the same dependence leads to an increase in thermal resistance parameters, such as heat deflection temperatures (HDTs) or Vicat temperatures. Previously, an inverse relationship between HDT and impact strength has been reported;[48,52,53] however, this was not observed in the present study. The results showed that as the crystallinity increased, so did both the HDT[54] and the impact strength, which has been previously reported for FDM-printed PLA composites.[26] Usually, a low softening point limits the range of application of PLA to 50−60 °C, which corresponds to the glass-transition region of its amorphous phase. The analysis of the DMA thermograms complements the DSC measurements in terms of changes in mechanical properties. As can be seen in Figure 13, in the glassy state, the highest value of storage modulus belongs to the injection-molded samples; similar values were reported for the printed samples after the annealing treatment. In the case of storage modulus, the initial room temperature values reflect the two dominant phenomena also observed in the previous analysis. The lowest values are observed for the samples prepared at the lowest range of printing parameters, respectively, the bed and melt temperatures. The apparent change occurs when both of the printing parameters are raised to higher values.

The importance of crystallinity becomes more evident at around 55 °C, when the majority of the tested samples reached the maximum deflection point in the HDT measurement (see

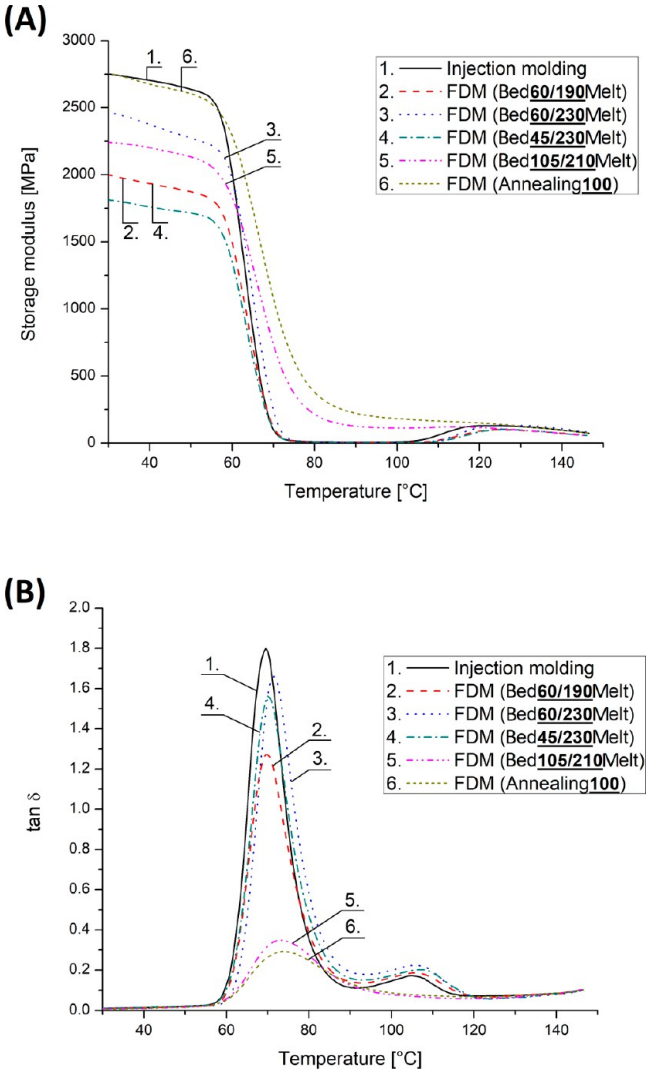

Figure 13. Thermograms of storage modulus (A) and tan δ (B) for samples obtained with different preparation methodologies.

Figure 14); this also applies to the injection-molded specimens. The difference in this aspect is in favor of the annealed samples.

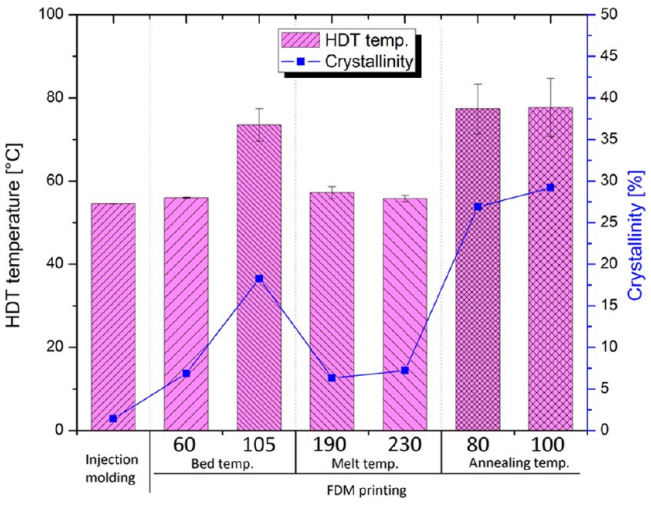

Figure 14. Comparison of HDTs and crystallinity levels for injection-molded samples and FDM-printed specimens.

DOI: 10.1021/acsomega.8b00129
ACS Omega 2018, 3, 4400−4411

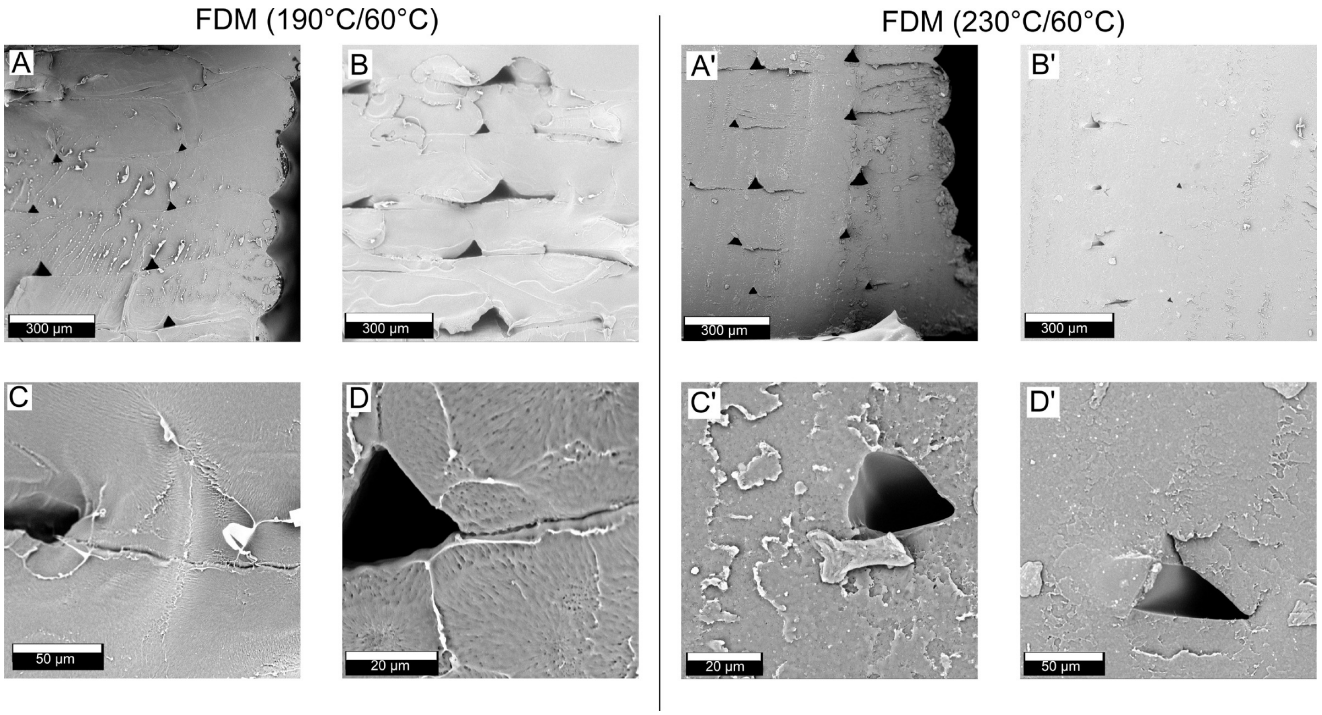

Figure 15. FDM-printed specimens at different melt temperatures. Structures of the sample cross sections showing the shell area (A, A′), raster area (B, B′), and enlargement of the void area (C, C′, D, and D′).

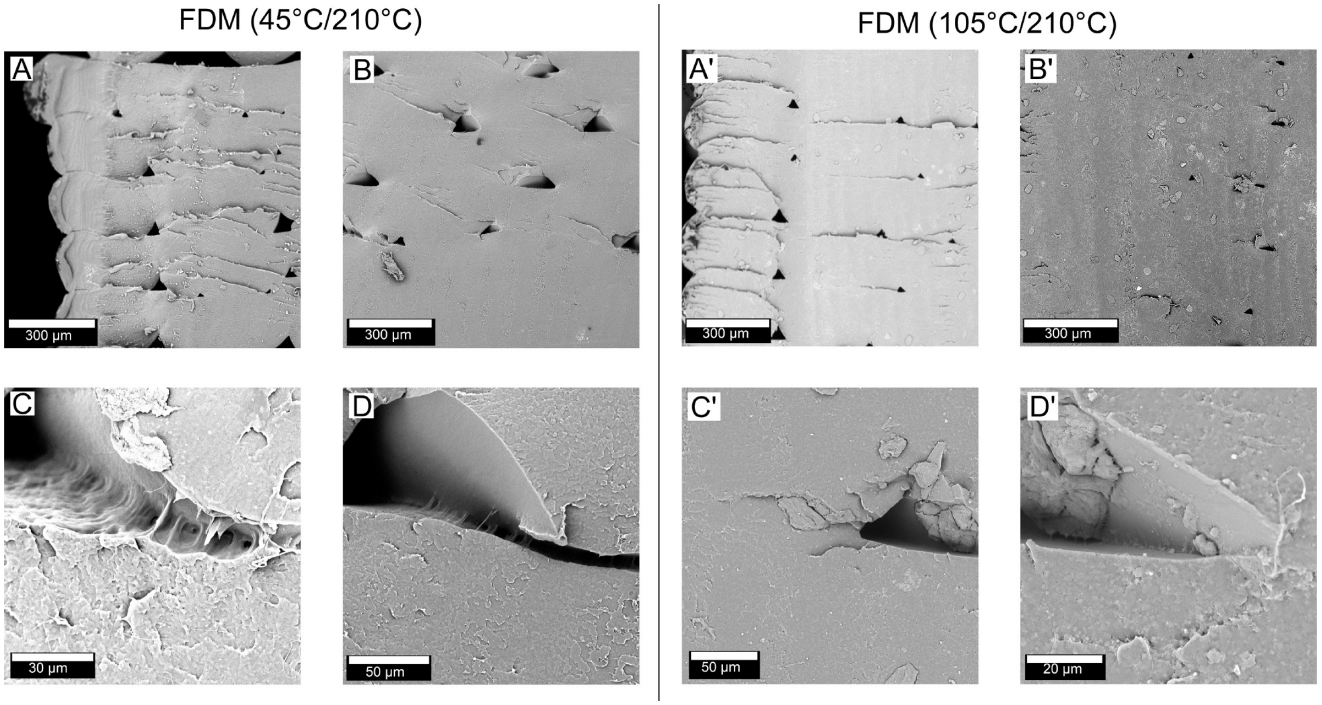

Figure 16. FDM-printed specimens at different bed temperatures. Structure of the sample cross sections showing the shell area (A, A′), raster area (B, B′), and enlargement of the void area (C, C′, D, and D′).

The highest HDT values were observed in both annealed samples. A significant increase was also observed for samples printed at the highest bed temperature (105 °C). Despite the difference in the initial value of storage modulus in both of these examples, the DMA thermograms have a very similar course, with apparently less reduction in stiffness at the relaxation stage, because of the lower content of the amorphous phase. This difference is particularly evident in the tan δ plots (Figure 13B), where for the samples printed at the highest bed temperature and the annealed samples, the additional cold crystallization peak does not occur, whereas for the rest of the samples it is clearly marked. This type of behavior has already been reported for PLA and its blends.[35,55]

Structure Evaluation. Some of the structural changes resulting from changes in crystallinity for selected samples can be easily assessed using thermal analysis. However, in the case

DOI: 10.1021/acsomega.8b00129
ACS Omega 2018, 3, 4400−4411

of tested samples, some trends of changes in mechanical properties cannot be correlated with the PLA phase morphology, particularly for samples printed with variable melt temperatures. In this case, the most important factor affecting the mechanical characteristics is the bonding strength between the individual layers of the printed material. For optimal selection of the parameters, the temperature of the polymer melt should allow partial melting of the previously applied layer. Under such conditions, diffusion is possible at the boundary of both printed layers, which in consequence not only provides better mechanical properties but also improves the surface quality of the printed model. Comparisons of samples printed at low and high nozzle temperatures reveal significant differences in the structure, which was reported previously for other FDM-printed polymers.[37,51]

For comparative purposes, cross sections of samples were presented both in the interior raster area of the specimen and on the edge of the sample where individual layers of filament form the so-called shell layer. In all printed samples, the outer layer of the sample is characterized by the large size of the trapezoidal holes. This indicates a rapid cooling of the material, which prevented the extruded filament from filling the free space of the model. However, the first significant differences can be observed by comparing the change in pore size within the interior of both samples. For low printing nozzle temperatures (Figure 15B), the size of the holes remained practically unchanged relative to that of the shell layer. In turn, for high printing nozzle temperatures, the pore size is significantly reduced in the raster area (Figure 15B′). Some similar trends were also reported in other studies.[12,40] However, considering the changes in the density of the samples, the apparent difference in pore size is not significantly influencing the total volume of voids, which should not significantly affect the mechanical properties. The more significant structural differences are visible within the joining lines of the individual layers of materials. A visible enlargement of the pore area suggests a clear lack of diffusion between filament layers for samples printed at 190 °C (see Figure 15C,D). A clear bonding line is visible throughout the structure of the entire model; thus, the reduced mechanical properties in this case are clearly due to the poor diffusion and lack of consistency between the individual layers of the filament.

Similar trends in structural changes can also be observed in the case of variable bed temperature. In this case, the pore size difference for the shell layer and raster area is even more visible. For samples printed at 105 °C, the viscosity of the already applied filament layers remains low enough to fill the free space of the model, leading to a nearly completely solid structure in the raster area, which is not possible for the outer/shell layer because of intensive heat exchange with the environment (Figure 16). A closer view at the void area also reveals some structural changes. As was observed with low nozzle temperatures, the reduction of the bed temperature also limits the diffusion process, leading to reduced interfacial adhesion between the printed layers.

CONCLUSIONS

By optimizing the printing parameters and with the introduction of post-print annealing, FDM samples of PLA were created with mechanical properties comparable and in some cases superior to those of their injection-molded counterparts. Variation in the melt temperature did not result in a significant change in the sample morphology; however, an increase in the bed temperature resulted in a large increase in crystallinity, providing a significant increase in the thermal resistance (HDT). From all of the mechanical characteristics, the impact strength was observed to be the most dependent on the degree of crystallinity, whereas the other tensile and flexural properties did not show such a significant improvement. However, increasing the bed temperature clearly improved both the modulus and strength of the samples. The 45/45° raster angle was consistently observed to be the ideal orientation of the filaments for optimal mechanical properties, though this factor seems to have a negligible impact. The observed changes allow us to conclude that in the case of FDM printing, the most favorable changes in thermomechanical properties of PLA-based samples are the result of post-processing annealing. Despite the necessity of using additional energy and time-consuming treatments, annealing of the finished elements has a significant advantage over applying high bed temperatures during the printing process. Post-processing allows the application of optimal printing conditions, which is important for improving the dimensional accuracy of models. In the presented studies, the main emphasis was placed on the improvement of mechanical properties. Hence, the bed temperature was mostly kept above the glass-transition temperature to maximize the bonding strength between deposited layers. The T_g value for PLA is around 60 °C, which results in fairly easy printing, even without a heated printing bed platform.

EXPERIMENTAL SECTION

Materials. The material used for all samples was a commercial PLA filament from polymaker(True Red PolyLite PLA). Like most of the commercially available materials, this PLA was supplied in the form of a bobbin with a wound filament line, with a diameter of 2.85 mm. Because of proprietary reasons, it was not known what nucleating agents or plasticizers were added, if any.

Sample Preparation. *Fused Deposition Modeling.* The fused layer modeling was performed using a LulzbotTaz 6 3D printer. Except the raster angle, all of the other machine parameters were kept constant, including a print speed of 50 mm/s, a travel speed of 200 mm/s, and a 100% fill density. The print time was also kept constant at 6.5 h for each variable printing parameter. Seven impact samples and five each of tensile and flexural samples were printed at a time. Painter's tape was laid out on the print surface for samples printed at bed temperatures of 90 and 105 °C to promote adhesion of the samples to the print surface.[6]

Injection Molding. Before injection molding, the filament was pelletized using a Reduction Engineering Bullet 64 pelletizer. After pelletizing, the pellets were dried for 16 h in the oven at 75 °C. Injection molding took place in a DSM 15cc micro compounder and injection molder following ASTM D3641 standards for PLA processing. The mold temperature was set at 30 °C, the barrel temperature at 180 °C, the injection pressure at 4 bar, and the hold pressure at 8 bar. Five flexural, five tensile, and seven impact samples were formed. Before testing, the samples were stored for 40 h at room temperature.

Annealing. To evaluate the effects of annealing on the mechanical properties of 3D printed models, it was decided to process only one type of prepared specimens. Before the annealing step, the samples were printed at a nozzle temperature of 210 °C and a bed temperature of 60 °C and a 45/45° raster angle and all other printing parameters were the

DOI: 10.1021/acsomega.8b00129
ACS Omega 2018, 3, 4400−4411

same as those in the previous prints. They were then annealed in the oven for 1 h, the first set of samples at 80 °C and the second at 100 °C.

Characterization. *Thermal Analysis (DSC, DMA, HDT).* Using TA Instruments DSC Q200, the thermal properties of the samples were studied. Two tests per sample were performed to create a standard deviation. Approximately, 5 mg was cut from each sample and was encapsulated in aluminum. With a 50 mL/min^{-1} nitrogen flow rate, the samples were ramped at 5.00 °C/min using a heat/cool/heat method. The crystallinity of the samples was calculated using the following formula

$$\% \text{ crystallinity} = X_c = 100 \times \frac{\Delta H_m - \Delta H_{cc}}{\Delta H_m^0} \quad (1)$$

where ΔH_m is the measured melting enthalpy, ΔH_{cc} is the measured enthalpy of cold crystallization, and ΔH_m^0 is the theoretical melting enthalpy of 100% crystalline PLA, taken from the literature to be 93.7 J/g[4].

Dynamic thermal analysis (DMA) was performed with the use of a DMA Q800 (TA Instruments, New Castle, DE). All measurements were carried out at a constant frequency of 1 Hz and strain amplitude of 0.01%. The temperature range was 30−150 °C, whereas the heating rate was 3 °C/min. The viscoelastic properties were collected from rectangular samples (3.2 × 12.7 × 50 mm) using the dual cantilever measurement mode.

The heat deflection temperature (HDT) of the samples was acquired using TA Instruments DMA Q800 following ASTM D648. The desired stress of 0.455 MPa was applied to the midsection of the sample, and a heating rate of 2 °C/min was utilized. The strain rate was measured at 250 μm (0.2% strain), and two tests were performed on each type of sample.

Measurements of Mechanical Properties (Tensile/Flexural/Notched Izod). The tensile and flexural testings were completed using an Instron 3382 Universal Testing Machine, following ASTM D638 and D790, respectively. The rate of the tensile testing crosshead speed was 5 mm/min, and the rate of the flexural testing crosshead speed was 14 mm/min. Before the samples were tested, they were stored at room temperature for 40 h after printing or injection molding. The impact testing was completed using a TMI 43-02 notched Izod impact tester with a 5 ft-lb hammer following ASTM D256. Before testing the samples, they were stored for 40 h after notching using a TMI notching cutter. Five samples were used in all tests to produce a standard deviation

Morphology, Density, and Viscosity of the Materials. The morphology of the fractured surface of notched Izod samples was investigated by a Phenom ProX SEM microscope using a 10 kV acceleration voltage. The surface of the samples was coated with a thin layer of gold. Density measurements were conducted using an MD300 densimeter (Alfa Mirage Co., Osaka, Japan) according to ASTM D792 standard methodology. Rheological measurements were conducted using an MCR 302 rheometer (Anton Paar GmbH, Graz, Austria). The configuration used was plate−plate geometry with a gap distance of 1 mm. The strain amplitude was set at 5%, and the angular frequency range was varied from 0.01 to 500 s^{-1}. Measurements were conducted under a nitrogen atmosphere at different temperatures from 190 to 230 °C, reflecting the melt temperatures selected for the printing process.

AUTHOR INFORMATION

Corresponding Authors

*E-mail: mmisra@uoguelph.ca (M.M.).
*E-mail: mohanty@uoguelph.ca (A.K.M.).

ORCID

Manjusri Misra: 0000-0003-2179-7699
Amar K. Mohanty: 0000-0002-1079-2481

Notes

The authors declare no competing financial interest.

ACKNOWLEDGMENTS

This research is financially supported by the Ontario Ministry of Agriculture, Food and Rural Affairs (OMAFRA), University of Guelph, Bioeconomy Industrial Uses Research Program Theme Project #030252; and the Natural Sciences and Engineering Research Council (NSERC), Canada Discovery Grants Project #400320.

REFERENCES

(1) Pearce, J. M.; Morris Blair, C.; Laciak, K. J.; Andrews, R.; Nosrat, A.; Zelenika-Zovko, I. 3-D Printing of Open Source Appropriate Technologies for Self-Directed Sustainable Development. *J. Sustainable Dev.* **2010**, *3*, 17−29.

(2) Huang, S. H.; Liu, P.; Mokasdar, A.; Hou, L. Additive Manufacturing and Its Societal Impact: A Literature Review. *Int. J. Adv. Manuf. Technol.* **2013**, *67*, 1191−1203.

(3) Bak, D. Rapid Prototyping or Rapid Production? 3D Printing Processes Move Industry towards the Latter. *Assem. Autom.* **2003**, *23*, 340−345.

(4) Harris, A. M.; Lee, E. C. Improving Mechanical Performance of Injection Molded PLA by Controlling Crystallinity. *J. Appl. Polym. Sci.* **2008**, *107*, 2246−2255.

(5) Wittbrodt, B.; Pearce, J. M. The Effects of PLA Color on Material Properties of 3-D Printed Components. *Addit. Manuf.* **2015**, *8*, 110−116.

(6) Wang, L.; Gramlich, W. M.; Gardner, D. J. Improving the Impact Strength of Poly(lactic Acid) (PLA) in Fused Layer Modeling (FLM). *Polymer* **2017**, *114*, 242−248.

(7) Saeidlou, S.; Huneault, M. A.; Li, H.; Park, C. B. Poly(lactic Acid) Crystallization. *Prog. Polym. Sci.* **2012**, *37*, 1657−1677.

(8) Li, H.; Huneault, M. A. Effect of Nucleation and Plasticization on the Crystallization of Poly(lactic Acid). *Polymer* **2007**, *48*, 6855−6866.

(9) Kousiatza, C.; Karalekas, D. In-Situ Monitoring of Strain and Temperature Distributions during Fused Deposition Modeling Process. *Mater. Des.* **2016**, *97*, 400−406.

(10) Gajdoš, I.; Slota, J. Influence of Printing Conditions on Structure in FDM Prototypes. *Teh. Vjesn.* **2013**, *20*, 231−236.

(11) Sood, A. K.; Ohdar, R. K.; Mahapatra, S. S. Parametric Appraisal of Mechanical Property of Fused Deposition Modelling Processed Parts. *Mater. Des.* **2010**, *31*, 287−295.

(12) Sun, Q.; Rizvi, G. M.; Bellehumeur, C. T.; Gu, P. Effect of Processing Conditions on the Bonding Quality of FDM Polymer Filaments. *Rapid Prototyping J.* **2008**, *14*, 72−80.

(13) Bellini, A.; Güçeri, S. Mechanical Characterization of Parts Fabricated Using Fused Deposition Modeling. *Rapid Prototyping J.* **2003**, *9*, 252−264.

(14) Young, D.; Kessler, J.; Czabaj, M. In *Interlayer Fracture Toughness of Additively Manufactured Unreinforced and Carbon-Fiber-Reinforced Acrylonitrile Butadiene Styrene*, Proceedings of the American Society for Composites - 31st Technical Conference, ASC 2016; DEStech Publications Inc.: Williamsburg, 2016.

(15) Durgun, I.; Ertan, R. Experimental Investigation of FDM Process for Improvement of Mechanical Properties and Production Cost. *Rapid Prototyping J.* **2014**, *20*, 228−235.

DOI: 10.1021/acsomega.8b00129
ACS Omega 2018, 3, 4400−4411

(16) Drummer, D.; Cifuentes-Cuéllar, S.; Rietzel, D. Suitability of PLA/TCP for Fused Deposition Modeling. *Rapid Prototyping J.* **2012**, *18*, 500−507.
(17) Chacón, J. M.; Caminero, M. A.; García-Plaza, E.; Núñez, P. J. Additive Manufacturing of PLA Structures Using Fused Deposition Modelling: Effect of Process Parameters on Mechanical Properties and Their Optimal Selection. *Mater. Des.* **2017**, *124*, 143−157.
(18) de Ciurana, J.; Serenóa, L.; Vallès, È Selecting Process Parameters in RepRap Additive Manufacturing System for PLA Scaffolds Manufacture. *Procedia CIRP* **2013**, *5*, 152−157.
(19) Tymrak, B. M.; Kreiger, M.; Pearce, J. M. Mechanical Properties of Components Fabricated with Open-Source 3-D Printers under Realistic Environmental Conditions. *Mater. Des.* **2014**, *58*, 242−246.
(20) Letcher, T.; Waytashek, M. In *Material Property Testing of 3D-Printed Specimen in Pla on an Entry-Level 3D Printer*, Proceedings of the ASME 2014 International Mechanical Engineering Congress and Exposition; ASME: Montreal, 2014; pp 1−8.
(21) Casavola, C.; Cazzato, A.; Moramarco, V.; Pappalettere, C. Orthotropic Mechanical Properties of Fused Deposition Modelling Parts Described by Classical Laminate Theory. *Mater. Des.* **2016**, *90*, 453−458.
(22) Song, Y.; Li, Y.; Song, W.; Yee, K.; Lee, K.-Y.; Tagarielli, V. L. Measurements of the Mechanical Response of Unidirectional 3D-Printed PLA. *Mater. Des.* **2017**, *123*, 154−164.
(23) Bellehumeur, C.; Li, L.; Sun, Q.; Gu, P. Modeling of Bond Formation Between Polymer Filaments in the Fused Deposition Modeling Process. *J. Manuf. Processes* **2004**, *6*, 170−178.
(24) Costa, S. F.; Duarte, F. M.; Covas, J. A. Estimation of Filament Temperature and Adhesion Development in Fused Deposition Techniques. *J. Mater. Process. Technol.* **2017**, *245*, 167−179.
(25) Abbott, A. C.; Tandon, G. P.; Bradford, R. L.; Koerner, H.; Baur, J. W. Process-Structure-Property Effects on ABS Bond Strength in Fused Filament Fabrication. *Addit. Manuf.* **2018**, *19*, 29−38.
(26) Kochesfahani, S. H. In *Improving PLA-Based Material for FDM 3D-Printers Using Minerals (Principles and Method Development)*, Proc. 54th SPE ANTEC, Indianpolis; 2016; pp 23−25.
(27) Jagenteufel, R.; Hofstaetter, T.; Kamleitner, F.; Pedersen, D. B.; Tosello, G.; Hansen, H. N. Rheology of High Melt Strength Polypropylene for Additive Manufacturing. *Adv. Mater. Lett.* **2017**, *8*, 712−716.
(28) Santana, L.; Lino Alves, J.; da Costa Sabino Netto, A. A Study of Parametric Calibration for Low Cost 3D Printing: Seeking Improvement in Dimensional Quality. *Mater. Des.* **2017**, *135*, 159−172.
(29) Wang, L.; Qiu, J.; Sakai, E. Microstructures and Mechanical Properties of Polylactic Acid Prepared by a Cold Rolling Process. *J. Mater. Process. Technol.* **2016**, *232*, 184−194.
(30) Madhavan Nampoothiri, K.; Nair, N. R.; John, R. P. An Overview of the Recent Developments in Polylactide (PLA) Research. *Bioresour. Technol.* **2010**, *101*, 8493−8501.
(31) Auras, R.; Harte, B.; Selke, S. An Overview of Polylactides as Packaging Materials. *Macromol. Biosci.* **2004**, *4*, 835−864.
(32) Sánchez, M. S.; Gómez Ribelles, J. L.; Hernández Sánchez, F.; Mano, J. F. On the Kinetics of Melting and Crystallization of Poly(l-Lactic Acid) by TMDSC. *Thermochim. Acta* **2005**, *430*, 201−210.
(33) Cocca, M.; Androsch, R.; Righetti, M. C.; Malinconico, M.; Di Lorenzo, M. L. Conformationally Disordered Crystals and Their Influence on Material Properties: The Cases of Isotactic Polypropylene, Isotactic poly(1-Butene), and Poly(l-Lactic Acid). *J. Mol. Struct.* **2014**, *1078*, 114−132.
(34) Righetti, M. C.; Gazzano, M.; Di Lorenzo, M. L.; Androsch, R. Enthalpy of Melting of A′- and α-Crystals of Poly(l-Lactic Acid). *Eur. Polym. J.* **2015**, *70*, 215−220.
(35) Tábi, T.; Hajba, S.; Kovács, J. G. Effect of Crystalline Forms (A′ and α) of Poly(lactic Acid) on Its Mechanical, Thermo-Mechanical, Heat Deflection Temperature and Creep Properties. *Eur. Polym. J.* **2016**, *82*, 232−243.
(36) Yasuniwa, M.; Tsubakihara, S.; Sugimoto, Y.; Nakafuku, C. Thermal Analysis of the Double-Melting Behavior of poly(L-Lactic Acid). *J. Polym. Sci., Part B: Polym. Phys.* **2004**, *42*, 25−32.
(37) Yang, C.; Tian, X.; Li, D.; Cao, Y.; Zhao, F.; Shi, C. Influence of Thermal Processing Conditions in 3D Printing on the Crystallinity and Mechanical Properties of PEEK Material. *J. Mater. Process. Technol.* **2017**, *248*, 1−7.
(38) Zhang, J.; Wang, X. Z.; Yu, W. W.; Deng, Y. H. Numerical Investigation of the Influence of Process Conditions on the Temperature Variation in Fused Deposition Modeling. *Mater. Des.* **2017**, *130*, 59−68.
(39) Seppala, J. E.; Hoon Han, S.; Hillgartner, K. E.; Davis, C. S.; Migler, K. B. Weld Formation during Material Extrusion Additive Manufacturing. *Soft Matter* **2017**, *13*, 6761−6769.
(40) Davis, C. S.; Hillgartner, K. E.; Han, S. H.; Seppala, J. E. Mechanical Strength of Welding Zones Produced by Polymer Extrusion Additive Manufacturing. *Addit. Manuf.* **2017**, *16*, 162−166.
(41) Dinwiddie, R. B.; Kunc, V.; Lindal, J. M.; Post, B.; Smith, R. J.; Love, L. J.; Duty, C. E. In *Infrared Imaging of the Polymer 3D-Printing Process*, Proceedings of SPIE - The International Society for Optical Engineering; Stockton, G. R., Colbert, F. P., Eds.; 2013.
(42) Compton, B. G.; Post, B. K.; Duty, C. E.; Love, L.; Kunc, V. Thermal Analysis of Additive Manufacturing of Large-Scale Thermoplastic Polymer Composites. *Addit. Manuf.* **2017**, *17*, 77−86.
(43) Henton, D.; Gruber, P.; Lunt, J.; Randall, J. Polylactic Acid Technology. In *Natural Fibers, Biopolymers, and Biocomposites*; CRC Press, 2005; pp 527−578.
(44) Perego, G.; Cella, G. D.; Bastioli, C. Effect of Molecular Weight and Crystallinity on Poly(lactic Acid) Mechanical Properties. *J. Appl. Polym. Sci.* **1996**, *59*, 37−43.
(45) Huang, T.; Yamaguchi, M. Effect of Cooling Conditions on the Mechanical Properties of Crystalline Poly(lactic Acid). *J. Appl. Polym. Sci.* **2017**, *134*, No. 44960.
(46) Aversa, C.; Barletta, M.; Gisario, A.; Pizzi, E.; Puopolo, M.; Vesco, S. Improvements in Mechanical Strength and Thermal Stability of Injection and Compression Molded Components Based on Poly Lactic Acids. *Adv. Polym. Technol.* **2017**, No. 21875.
(47) Wei, Z.; Song, P.; Zhou, C.; Chen, G.; Chang, Y.; Li, J.; Zhang, W.; Liang, J. Insight into the Annealing Peak and Microstructural Changes of Poly(l-Lactic Acid) by Annealing at Elevated Temperatures. *Polymer* **2013**, *54*, 3377−3384.
(48) Vadori, R.; Mohanty, A. K.; Misra, M. The Effect of Mold Temperature on the Performance of Injection Molded Poly(lactic Acid)-Based Bioplastic. *Macromol. Mater. Eng.* **2013**, *298*, 981−990.
(49) Armillotta, A.; Bellotti, M.; Cavallaro, M. Warpage of FDM Parts: Experimental Tests and Analytic Model. *Rob. Comput. Integr. Manuf.* **2018**, *50*, 140−152.
(50) Weng, Z.; Wang, J.; Senthil, T.; Wu, L. Mechanical and Thermal Properties of ABS/montmorillonite Nanocomposites for Fused Deposition Modeling 3D Printing. *Mater. Des.* **2016**, *102*, 276−283.
(51) Cicala, G.; Latteri, A.; Del Curto, B.; Lo Russo, A.; Recca, G.; Farè, S. Engineering Thermoplastics for Additive Manufacturing: A Critical Perspective with Experimental Evidence to Support Functional Applications. *J. Appl. Biomater. Funct. Mater.* **2017**, *15*, 10−18.
(52) Nagarajan, V.; Zhang, K.; Misra, M.; Mohanty, A. K. Overcoming the Fundamental Challenges in Improving the Impact Strength and Crystallinity of PLA Biocomposites: Influence of Nucleating Agent and Mold Temperature. *ACS Appl. Mater. Interfaces* **2015**, *7*, 11203−11214.
(53) Nagarajan, V.; Mohanty, A. K.; Misra, M. Perspective on Polylactic Acid (PLA) Based Sustainable Materials for Durable Applications: Focus on Toughness and Heat Resistance. *ACS Sustainable Chem. Eng.* **2016**, *4*, 2899−2916.
(54) Battegazzore, D.; Bocchini, S.; Frache, A. Crystallization Kinetics of Poly(lactic Acid)-Talc Composites. *eXPRESS Polym. Lett.* **2011**, *5*, 849−858.
(55) Yang, T. C.; Hung, K. C.; Wu, T. L.; Wu, T. M.; Wu, J. H. A Comparison of Annealing Process and Nucleating Agent (Zinc Phenylphosphonate) on the Crystallization, Viscoelasticity, and Creep Behavior of Compression-Molded Poly(lactic Acid) Blends. *Polym. Degrad. Stab.* **2015**, *121*, 230−237.

DOI: 10.1021/acsomega.8b00129
ACS Omega 2018, 3, 4400−4411